

## Article

# Synergistic Effect of Structure and Morphology of ZSM-5 Catalysts on the Transformation of Methanol to Propylene

Wei Zhang <sup>1,2</sup>, Kangzhou Wang <sup>3</sup>, Xinhua Gao <sup>4,\*</sup> , Xiaojing Yong <sup>2</sup> and Yanlong Gu <sup>1,\*</sup>

<sup>1</sup> Key Laboratory of Material Chemistry for Energy Conversion and Storage, Ministry of Education, Hubei Key Laboratory of Material Chemistry and Service Failure, School of Chemistry and Chemical Engineering, Huazhong University of Science and Technology, Wuhan 430074, China

<sup>2</sup> National Energy Group Ningxia Coal Industry Co., Ltd., Yinchuan 750411, China

<sup>3</sup> School of Materials and New Energy, Ningxia University, Yinchuan 750021, China

<sup>4</sup> State Key Laboratory of High-Efficiency Utilization of Coal and Green Chemical Engineering, College of Chemistry & Chemical Engineering, Ningxia University, Yinchuan 750021, China

\* Correspondence: gxm@nxu.edu.cn (X.G.); klgyl@hust.edu.cn (Y.G.)

**Abstract:** Here, the efficient synthesis of propylene from methanol was achieved using a series of HZSM-5 catalysts. The effect of the structure and morphology of ZSM-5 on the conversion of methanol to propylene was studied. The structure and physicochemical properties of the synthesized catalysts were analyzed by multiple characterization techniques. The characterization results revealed that the alumina content rationally modified the acid properties of ZSM-5. When using a ZSM-5 catalyst with a hexagonal single crystal and a Si/Al ratio of 177, the selectivity of propylene reached 39.7% at 480 °C. Furthermore, the formation of methane was reduced. This provides a clue for catalyst design to enable the selective transformation of methanol into propylene.

**Keywords:** methanol; hydrocarbon; acidity; pore distribution; synergistic effect



**Citation:** Zhang, W.; Wang, K.; Gao, X.; Yong, X.; Gu, Y. Synergistic Effect of Structure and Morphology of ZSM-5 Catalysts on the Transformation of Methanol to Propylene. *Catalysts* **2024**, *14*, 67. <https://doi.org/10.3390/catal14010067>

Academic Editors: Lei Liu, Zhijun Zuo and Jose Maria Arandes

Received: 7 November 2023

Revised: 8 January 2024

Accepted: 9 January 2024

Published: 15 January 2024



**Copyright:** © 2024 by the authors. Licensee MDPI, Basel, Switzerland. This article is an open access article distributed under the terms and conditions of the Creative Commons Attribution (CC BY) license (<https://creativecommons.org/licenses/by/4.0/>).

## 1. Introduction

Methanol can undergo dehydration condensation, alkylation, oligomerization, cracking, cleavage, aromatization and other reactions when catalyzed by acidic zeolite molecular sieves, resulting in a wide product distribution [1]. Because molecular sieves have variable acidity and diverse structures, it is possible to control the product distribution. Pore size is a key factor in controlling product distribution, such as via SAPO-34 molecular sieve-catalyzed methanol conversion [2,3], which produces low-carbon olefins, while ZSM-5 produces a mixture of products dominated by propylene, which is known as the MTP process [4]. At present, propylene is primarily produced from oil refineries, however, coal-based MTP is also commercialized as an alternative approach. The MTP reaction is generally catalyzed by ZSM-5, which has unique surface and structure properties [5]. For example, the acidic nature of ZSM-5 molecular sieves has an important influence on the product distribution [6,7]. In general, the product of methanol conversion is dominated by aromatics and alkanes when the acid density is high, while the product is dominated by olefins when the acid density is low [8]. Furthermore, the combined presence of Brønsted acid sites and Lewis acid sites may improve the catalytic performance of molecular sieves [9,10].

The effect of molecular sieve pore size on product distribution is often referred to as “shape selectivity”; i.e., differences in the shape and size of reactants, intermediates, or reaction products lead to inconsistent spatial constraints on the formation and diffusion of different compounds, which in turn affect the product distribution [11,12]. In addition to the spatial constraints arising from the intrinsic pore size of molecular sieves, many reports have observed the effect of pore length on the composition of substances in the reaction mixture during the study of molecular sieve morphology; i.e., the diffusion effect arising

from the pore length of molecular sieves can also change the product distribution [13,14]. Moreover, the deactivation of acidic zeolite catalysts by coking during methanol conversion is non-negligible [15]. Therefore, for a specific molecular sieve-catalyzed conversion process, it is possible to maximize the target product yield through the combined control of surface properties and morphology.

In the present work, two series of HZSM-5 catalysts with different morphology—ellipsoidal agglomerates and hexagonal single crystals—were synthesized via the hydrothermal method. In each series, prepared HZSM-5 catalysts with different acidity and pore distribution were achieved by the control of the Si/Al ratio in the precursors. The synergistic effect of surface and pore structure on the catalytic performance of methanol during conversion to propylene was studied.

## 2. Results and Discussion

### 2.1. Structural and Morphology Analysis

The X-ray diffraction patterns of the two series of molecular sieve samples are shown in Figure 1. There were five diffraction peaks at  $2\theta = 7.9^\circ, 8.8^\circ, 23.1^\circ, 23.8^\circ,$  and  $24.4^\circ$ , due to the inherent MFI topology structure [16]. Moreover, there were no obvious other peaks, indicating that each sample was a well-crystallized MFI pure phase. Furthermore, characteristic diffraction peaks of all as-prepared zeolites were basically consistent, with the decrease of alumina content, indicating that altering the Si/Al ratio of samples could not significantly influence the zeolite structure.

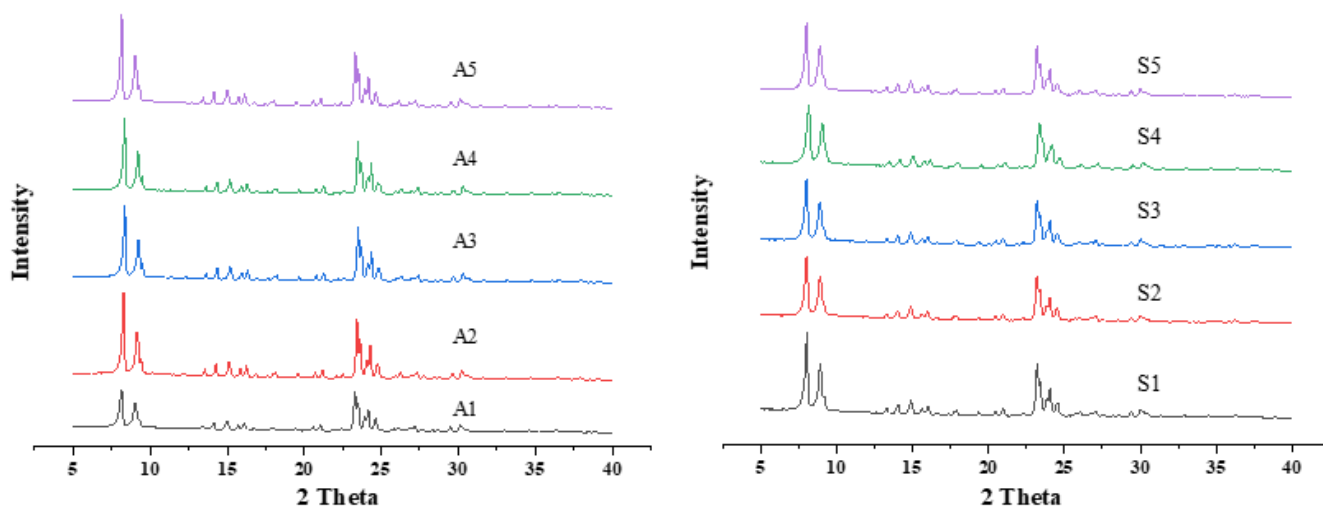
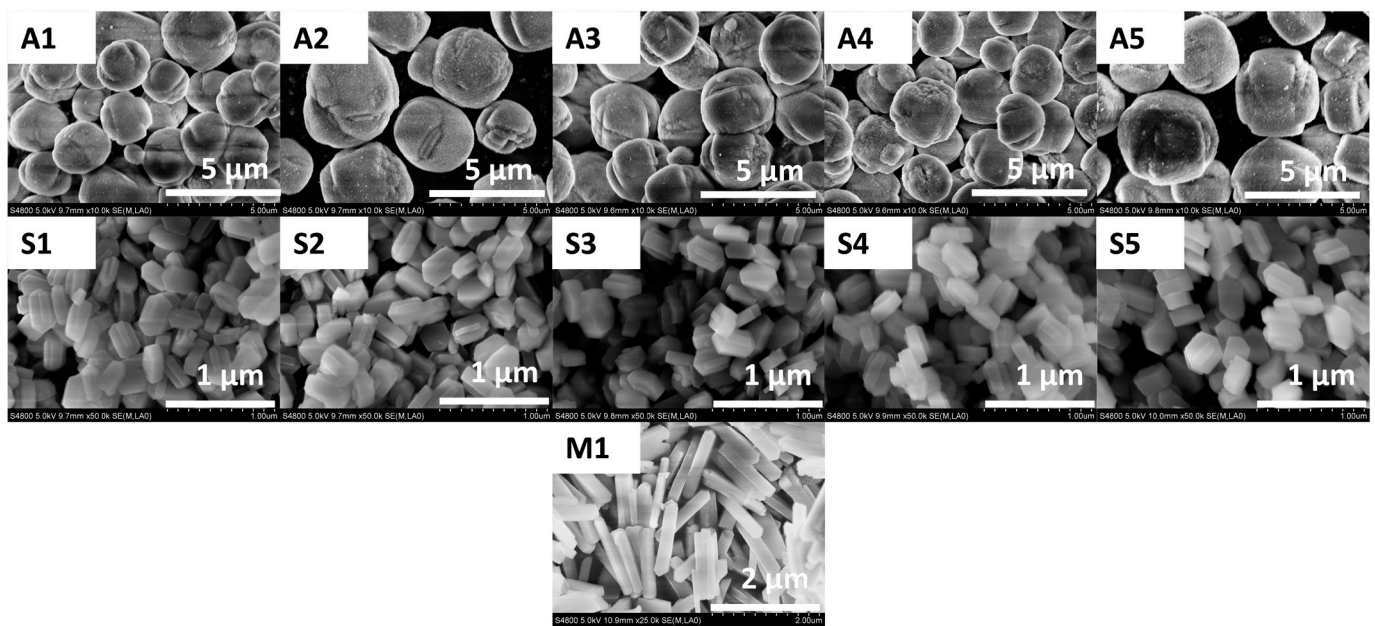


Figure 1. XRD patterns of as-prepared zeolite.

From the SEM photographs (Figure 2), it can be seen that the appearance of samples A1–A5 was relatively similar, like an ellipsoidal shape; there were no obvious crystal angles, and the surface of the sphere was granular, which was tentatively judged to be formed by particle agglomeration. The particle sizes of each sample after agglomeration were slightly different; A2 and A5 were slightly larger in size, about  $3\ \mu\text{m}$ , and A1, A3, and A4 particles were about  $2\ \mu\text{m}$  in size. S1–S5 had a hexagonal single-crystal appearance, with a long side size of about  $500\ \text{nm}$  and a thickness of about  $100\ \text{nm}$ . The sample M1 had a bar shape with a length of about  $1.6\ \mu\text{m}$ .



**Figure 2.** SEM images of the as-synthesized catalysts.

### 2.2. Textural Properties

Mercury injection test can be used to examine the properties of volume and pore size distribution of mesopores and macropores of solid materials [17]. The principle is that liquid mercury will fill into the pores of the material sequentially, from large to small, under the effect of gradually increasing external pressure [18]. In this paper, three samples from each of the two groups were tested for mercury compression, and the results are shown in Figures 3 and 4.

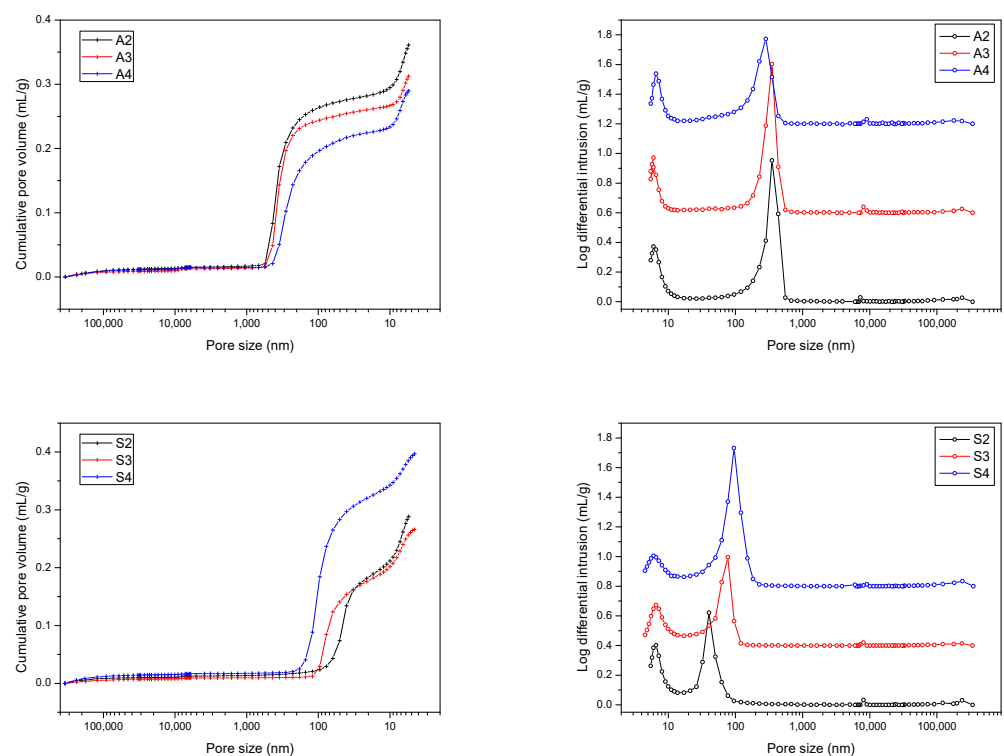


**Figure 3.** Pore volume and pore distribution of the as-prepared catalysts from mercury injection tests.

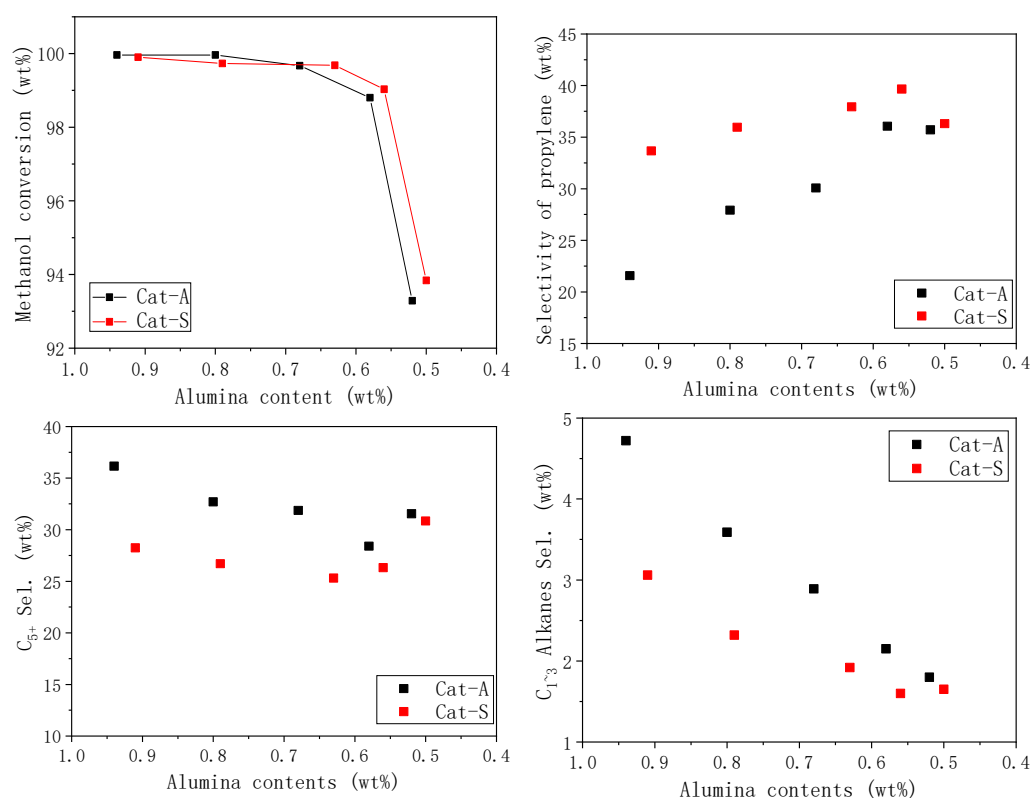


**Figure 4.** The trend of methanol conversion, propylene selectivity, and by-product selectivity changed with alumina content.

The left panel of Figure 3 shows the trend of cumulative pore volume with pore diameter. The content of alumina from A2 to A4 gradually decreased (Si/Al ratio increased), and the cumulative pore volume decreased, indicating that the product tended to be dense. The right panel, by differentiating and taking the logarithm of the liquid mercury squeezing volume and plotting the pore diameter distribution, clearly shows that the pore diameter distribution of the three samples was similar, and they all contained mesopores of 5–6 nm and macropores of more than 300 nm, among which the pore diameter of A4 was slightly smaller than that of the other two samples, and the distribution was wider. A comprehensive analysis of the mercury-pressure experimental data and the appearance of the samples showed that there was a correlation between the two. The mesopores of the samples should arise from the interstices of the microcrystal stacking within the agglomerates, while the macropores arise from the interstices between the agglomerate particles [19]. The agglomerate size of A4 was slightly smaller than that of the other two samples, and thus the macropore pore size was also slightly smaller.

The cumulative pore volume trends of the hexagonal single crystal samples with alumina content differed significantly from those of the agglomerate products, and the pore volume of sample S4, which had a lower alumina content, was significantly larger than that of the other two samples. As for the pore size distribution, the liquid mercury-filled peaks of mesopores and macropores appeared in all samples, and the mesopore pore size was comparable to that of the agglomerate samples, which was about 5–6 nm; the macropore size was significantly smaller than that of the agglomerate samples, with a distribution range of 30–100 nm; in addition, the macropore pore size became larger as the alumina content of the samples decreased. The large pore size of the hexagonal single-crystal sample was more consistent with its appearance and morphology, because its particle size was 100–500 nm, and the pore size of 30–100 nm formed by crystal stacking was more reasonable. The larger pore size with decreasing alumina content of the sample may have been caused by the different degrees of twin eutectics of the sample. This can

be observed from the SEM photographs with the increasing trend of twin eutectics with increasing alumina content, which therefore led to a more dense molecular sieve crystal stacking. Alternatively, the mesopores with size at 5–6 nm detected in the mercury injection tests may have been produced by the dehydration of alumina gel which was used as an adhesive in the kneading process.

The pore structure data measured by nitrogen adsorption experiments are shown in Table 1. We calculated 363–452 m<sup>2</sup>/g of total surface area for each sample by the BET method. The lowest value of surface area calculated by the T-plot method reached 346 m<sup>2</sup>/g, which was a good value for the MFI structured molecular sieve material, indicating that the molecular sieve material used for the study was well crystallized and had permeable pore channels, making it conducive to the diffusion of gas molecules. Comparing the values of the two series samples with each other, it can be found that the total specific surface area of the agglomerated series samples was higher. The increase in specific surface area was mainly represented by the microporous surface area by the T-plot method; the approximate mesoporous specific surface area data were obtained by the difference between the BET method and the T-plot method, and the mesoporous specific surface area of the agglomerated series samples was also slightly higher than that of the hexagonal single crystal series samples. Additionally, the sample M1 had a little lower specific surface area than the other samples. For the pore volume data, there was little difference among all the samples. The pore volume was about 0.20 cm<sup>3</sup>/g.

**Table 1.** Alumina content and pore properties of the catalysts.

Samples	Si/Al Ratio	Surface Area (BET), m <sup>2</sup> /g	Surface Area (T-plot), m <sup>2</sup> /g	Surface Area (Mesopore), m <sup>2</sup> /g	Pore Volume, cm <sup>3</sup> /g
A1	105	437	390	47	0.21
A2	124	444	404	40	0.19
A3	143	448	401	47	0.20
A4	171	452	401	51	0.20
A5	195	447	399	48	0.20
S1	110	400	357	43	0.21
S2	125	395	353	42	0.20
S3	157	404	366	38	0.20
S4	177	397	384	15	0.19
S5	199	410	383	27	0.21
M1	152	363	346	17	0.20

The aluminum–oxygen tetrahedra in the structure of silica–aluminum molecular sieves were negatively charged and thus could adsorb hydrogen protons and thus produce acidity; therefore, the acidity of well-crystallized molecular sieve materials is mainly determined by the aluminum content [20]. The alumina content of the materials used is listed in Table 1 and varied from 0.50 to 0.94%, corresponding to a ratio of silica to alumina from about 100 to 200.

### 2.3. Catalytic Performance

Table 2 lists the methanol conversion and hydrocarbon product distribution data obtained for each molecular sieve catalyst in the catalytic performance evaluation. Each value is the average value obtained from multiple sampling analyses over a 24 h period.

The conversion of methanol to hydrocarbon products involves a series of acid-catalyzed reactions, and the methanol conversion rate is closely related to the strength of the catalyst acidity. Comparing the data in Table 2, it can be found that most of the samples achieved close to 100% methanol conversion; however, when the alumina content decreased to a certain level, the methanol conversion of both morphologies of the molecular sieve catalysts decreased, indicating that the catalysts were less active and less acidic. However, the methanol conversion rate of the catalysts prepared from different morphologies of molecu-

lar sieves was not completely consistent, with the methanol conversion of the agglomerate morphology (Cat-A) being slightly higher than that of the hexagonal single crystal (Cat-S) when the alumina content was higher, while the conversion of the agglomerate samples was lower when the alumina content was low and the catalyst activity was insufficient (see Figure 5).

**Table 2.** Results of the methanol conversion test.

Catalyst	Conv. /wt%	Selectivities/wt%						
		Methane	Ethylene	Ethane	Propylene	Propane	C <sub>4</sub>	C <sub>5+</sub>
Cat-A1	99.96	1.06	11.34	0.19	21.57	3.47	26.21	36.16
Cat-A2	99.96	1.02	10.75	0.18	27.92	2.39	25.05	32.69
Cat-A3	99.67	0.95	9.71	0.12	30.07	1.81	25.46	31.87
Cat-A4	98.80	0.87	8.48	0.08	36.06	1.20	24.90	28.41
Cat-A5	93.29	0.83	6.96	0.06	35.71	0.92	23.99	31.54
Cat-S1	99.90	1.20	10.79	0.16	33.67	1.70	24.24	28.24
Cat-S2	99.73	1.01	9.66	0.10	35.96	1.21	25.37	26.70
Cat-S3	99.68	0.68	9.56	0.07	37.93	1.16	25.28	25.31
Cat-S4	99.03	0.59	7.95	0.06	39.66	0.95	24.47	26.32
Cat-S5	93.84	0.67	7.28	0.06	36.31	0.92	23.92	30.84
Cat-M1	99.43	1.11	7.29	0.07	36.63	0.96	24.56	29.36

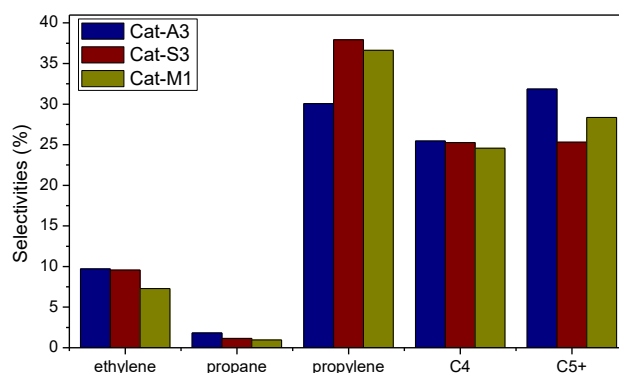


**Figure 5.** Products' distribution across samples with different morphology.

The propylene selectivity of both groups of samples showed an increase followed by an increase in the ratio of silica to alumina; however, the selectivity values differed significantly. In the examined alumina content range, the propylene selectivity of the hexagonal monocrystal series catalysts always remained above 30%, while the lowest value of propylene selectivity of the agglomerate samples was only 21.57%, and the highest value of selectivity also differed by more than 3% compared to that of the hexagonal monocrystal. Although the selectivity to propylene was not high enough compared to that of other ZSM-5 molecular sieves (30–50%) [12], the highest propylene selectivity also reached 39.66% in Cat-S4.

#### 2.4. Structure–Performance Relationship

The conversion process of methanol in an acidic molecular sieve consists of multiple reactions [21]. Firstly, there is the reversible conversion of methanol and dimethyl ether, which is a fast reaction; secondly, there is the conversion of methanol/dimethyl ether to low-carbon olefins, which is based on the hydrocarbon pool mechanism and requires the generation of transition state intermediates before achieving this reaction, resulting in a certain induction period and is a slow reaction [22]. Finally, there is the conversion of olefin products into various by-products catalyzed by molecular sieve, including oligomerization, alkylation, cracking, aromatization, and other processes [23]. In industrial applications,

it is expected to maximize the selectivity of propylene, which requires the modulation of catalyst acid properties to achieve high conversion of methanol, and meanwhile the optimal control of the side reactions of olefins.

During the catalytic performance testing, we observed that the methanol conversion showed a decreasing trend with the decrease of alumina content in both groups of samples, which indicated that the acid strength and catalytic activity of the catalysts plays important role is the transformation of methanol. At the same time, all kinds of side reactions were suppressed, the most obvious one being the significant reduction of alkane production, and the total selectivity of methyl, ethyl, and propane of the agglomerate samples decreased from 4.72% to 1.80%, with a total decrease of 61.9%. Olefins underwent hydrogen transfer reactions to produce aromatics and alkanes, from which it can be assumed that the hydrogen transfer reactions were inhibited and the aromatic selectivity decreased more substantially as the catalyst became less acidic.

The  $C_{5+}$  hydrocarbon products are produced by oligomerization, aromatization, and alkylation reactions [24]. As the catalyst acidity decreased, the activity of these side reactions decreased, thus making the total selectivity of  $C_{5+}$  products decrease. However, this selectivity turned to an increasing trend after dropping to a certain low value, which can be attributed to the decay of cracking reactions caused by insufficient catalyst acidity. The consumption of  $C_{5+}$  hydrocarbon products decreased, and this pattern occurred under the combined effect of several types of side reactions.

Ethylene selectivity also tended to decrease with decreasing catalyst acidity, indicating that the sources of ethylene in the products were diverse, that cracking produced ethylene and was an important part of the source of ethylene [25], and that weakening of the cracking reaction leads to a decrease in ethylene selectivity. In addition, the change in the  $C_4$  selectivity showed an overall decreasing trend consistent with ethylene, but the decrease was small, indicating that its production and consumption were less affected by catalyst acidity within the acidity range examined.

Above, we found that the variation in the acidity of the ZSM-5 molecular sieve catalysts significantly affected the product distribution of the methanol conversion, with weaker acid strengths inhibiting the side reactions and thus substantially improving the selectivity of the target product, propylene. However, we also observed that molecular sieve catalysts with similar acid strength (similar molecular sieve alumina content) exhibited very different propylene selectivity due to their inconsistent morphology; e.g., Cat-S1 showed 1.5 times higher propylene selectivity than Cat-A1.

A detailed comparison of the product distributions of Cat-S1 and Cat-A1 (see Table 3) showed that Cat-A1 produced more by-products, mainly  $C_{5+}$ ,  $C_4$ , and propane, with the largest increase in  $C_{5+}$ . When we divided the selectivity difference of each product between the two catalyst samples and the selectivity value of Cat-S1 to calculate the change, we found that the increase in propane was particularly prominent. The increase was particularly significant for propane. Based on the characteristics of the reaction in the system, the product of alcohol–ether dehydration should be an olefin or cycloalkane with a carbon-to-hydrogen ratio of 1:2 before the hydrogen transfer reaction and the aromatization based on it; therefore, the significant increase in propane selectivity indicated a more intense hydrogen transfer reaction in Cat-A1. The two catalyst samples used for comparison had similar acid intensities, which allowed us to determine that the diffusion factor, i.e., the difference in steric hindrance within the catalyst, played a more critical role in the reaction.

During the characterization of crystal phase and pore system, we found that both groups of samples were well crystallized, with a large specific surface area and relatively abundant mesopores and macropores. Therefore, compared with the slow diffusion and mass transfer rate inside the ZSM-5 molecular sieve crystal, the extra-crystal diffusion resistance was small and the effect on the catalytic reaction can be neglected. Thus, the intra-crystal diffusion limitation should be the main reason for the large difference in propane selectivity. Although propane can diffuse into and out of the pore system of zeolite ZSM-5 freely based on its small molecular size, the generation of propane inside the channel

of zeolite crystal can still be limited because the reaction that produces propane requires the participation of multiple molecules or large molecular compounds, which have difficulties in reaching the active centers in the pore channels because of the pore-confined effect. Thus, the production of propane is inhibited. The hexagonal single-crystal morphology of S1 had longer intracrystalline pore channels and stronger inhibition of propane. As a result, less propane was produced by Cat-S1 due to its relatively fewer active sites on the surface available for those side reactions.

**Table 3.** Comparison of Cat-S1 and Cat-A1 and their product distribution.

Catalyst	Selectivities/wt%						
	Methane	Ethylene	Ethane	Propylene	Propane	C <sub>4</sub>	C <sub>5+</sub>
Cat-S1	1.20	10.79	0.16	33.67	1.70	24.24	28.24
Cat-A1	1.06	11.34	0.19	21.57	3.47	26.21	36.16
Diff.	−0.16	0.55	0.03	−12.10	1.77	1.97	7.92
Relative Diff./%	−13.3	5.1	18.8	35.9	104.1%	8.1%	28.0%

The formation of the C<sub>5+</sub> with the larger molecular size was also affected by the pore-confined domain-limiting effect [26], thus Cat-S1 obtained lower selectivity of the C<sub>5+</sub> than Cat-A1. It is worth noting that the cracking reaction in the system can consume large-molecule compounds to produce low-carbon hydrocarbons. The cracking reaction in Cat-A1 was less affected by intracrystalline diffusion and had higher activity; however, it did not obtain lower selectivity to C<sub>5+</sub> products, indicating that the consumption of the cracking reaction was not enough to offset the increased production of the C<sub>5+</sub> and the inhibition of the domain-limiting effect dominated.

The comparison of the catalytical performances of Cat-A1 and Cat-S1 shows that the pore-confined effect played a significant role in suppressing side reactions of methanol to hydrocarbons in the case of excessive activity. In fact, this effect also worked when the activity decreased to a moderate degree. Here, three catalysts that had close alumina contents were selected for study, so as to obtain a deep understanding of the pore-confined effect in methanol-to-hydrocarbons process. These catalysts have distinct microstructures, and the strength of steric hindrance decreased reasonably in the order: Cat-M1 > Cat-S3 > Cat-A3.

Figure 5 shows the product distribution of the chosen catalysts. We can see that selectivity to ethylene, propane, and C<sub>4</sub> hydrocarbons decreased with the increase in strength of pore-confined effect, which conforms to the rule mentioned above. Surprisingly, Cat-S3 showed the highest selectivity to propylene and the lowest to C<sub>5+</sub> hydrocarbons. This result is predictable if we take the cracking reaction into consideration. The cracking of C<sub>5+</sub> hydrocarbons is a side reaction benefit that can produce propylene and help to reach a higher selectivity to propylene, as expected. The enhanced pore-confined effect of Cat-M1 led to a weakened cracking reaction, thus producing less propylene than Cat-S3, and correspondingly more C<sub>5+</sub> hydrocarbons remained.

In addition, the intracrystalline diffusion limitation also had an effect on the conversion of methanol [27]. Figure 4 shows that the methanol conversion did not reach 100% when the catalyst activity was sufficient (alumina content >0.7%), and the conversion of the hexagonal single crystal series samples was slightly lower than that of the agglomerate samples, indicating that the inter-crystalline diffusion limitation reduced the chance for methanol and dimethyl ether to contact with the catalytic active sites.

The acid properties of the catalysts are shown in Figure 6. There are two desorption peaks at temperature ranges of 100–250 °C and 250–450 °C, which generally relate to the weak acid and strong acid sites, respectively. As reported, the catalytic performance not only related to the strength but was also influenced by the type of acid sites. At present, Brønsted acid sites are believed to be the active sites for olefin production [12]. In the present work, the selectivity to propylene obviously increased with decreasing amounts of both weak and strong acid. Furthermore, it is clear that with the decrease of alumina

content, both weak acid and strong acid strength of the zeolite decreased, which is beneficial for the delaying of coke formation [28,29]. As mentioned above, by modulating the content of alumina in the ZSM-5 molecular sieve, we can obtain molecular sieve catalysts with suitable acid strength, which can suppress side reactions; while changing the molecular sieve morphology and strengthening the influence of intra-crystal diffusion in the molecular sieve can further suppress the related side reactions. Thus, higher selectivity of propylene was produced. Similarly, the strength of the pore-confined effect should moderate just like the acidity to achieve high conversion of methanol, acceptable cracking activity, and well-inhibited side reactions spontaneously. Moreover, the lower Si/Al will lead to faster formation of methylated aromatic species, then increase the coking rates [12]. It is also believed that the coking of H-ZSM-5 during MTP does not proceed in the pores but on the crystallites surface [15]. Overall, propylene selectivity and resistance to coking are the two most important parameters in catalysts. Therefore, in order to maximize the propylene yield, the catalyst design should include the optimization in both aspects in order to achieve better application results.

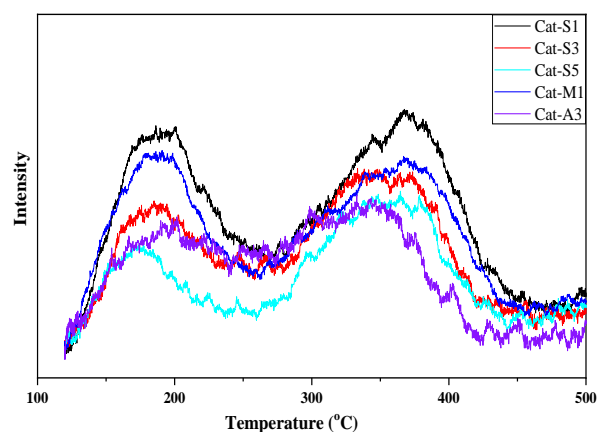


Figure 6.  $\text{NH}_3$ -TPD curves of the catalysts.

### 3. Experiments

#### 3.1. Catalyst Preparation

The ZSM-5 samples used in this study were divided into two series, ellipsoidal agglomerates and hexagonal single crystals, based on the differences in morphology, and each series contained five samples with different aluminum contents. A commercial zeolite ZSM-5 from the company Novel (Zhuoyue Environmental Protection New Materials, Shanghai, China) with a size of about 1 micron was used for comparison.

Ellipsoidal agglomerate samples were prepared using a silica source of silica sol, an alumina source of aluminum sulfate hexadecahydrate, a structure directing agent of tetrapropylammonium bromide (TPABr), and sodium hydroxide to mediate the alkalinity, with the following ratios of material amounts of the synthetic precursors:  $\text{SiO}_2:\text{Al}_2\text{O}_3:\text{TPA}^+:\text{OH}^-:\text{H}_2\text{O} = 1:x:0.25:0.2:15$ . After the precursor preparation was completed, the product was crystallized at 170 °C for 16 h under stirring and categorized into A1, A2, A3, A4 and A5 according to the high-to-low alumina content. Hexagonal single crystal samples were prepared using a silica source of silica sol, an alumina source of aluminum sulfate hexadecahydrate and a structural directing agent of tetrapropylammonium hydroxide (TPAOH) with the following ratios of material amounts of synthetic precursors:  $\text{SiO}_2:\text{Al}_2\text{O}_3:\text{TPA}^+:\text{H}_2\text{O} = 1:x:0.25:0.2:30$ . After the preparation of the precursor system, the product was crystallized at 170 °C for 16 h with stirring, and the products were categorized into S1, S2, S3, S4 and S5 according to the high-to-low alumina content. The commercial zeolite ZSM-5 was named M1.

Before being used for catalytic performance testing, the ZSM-5 molecular sieves needed to be calcined to remove the organic structure directing agent. Then, the calcined samples were treated with ammonium-ion exchange in order to form hydrogen-type zeolites. The ammonium-ion exchange feed mass ratios: molecular sieve: $\text{NH}_4\text{Cl}:\text{H}_2\text{O} =$

1:0.05:10. The exchanging mixture was kept at 95 °C for 2 h; the material after ammonium ion exchange was filtered, washed and dried, and then calcined to remove ammonia to obtain hydrogen-type zeolite; subsequently, the obtained product was mixed and kneaded with the pseudo-boehmite and dilute nitric acid (nitric acid mass concentration of 5%) in the mass ratio of 1:0.2:0.9, and extruded by screw extruder to obtain strips of 3 mm in diameter, which were then dried, calcined, and crushed into 20~40 mesh particles. The catalyst samples were named by adding the prefix Cat in front of the molecular sieve number; e.g., Cat-A1.

### 3.2. Characterization

The crystal phase analysis of the molecular sieve material was performed on an X-ray diffractometer from the company PANalytical, model XPert3 Powder (Malvern, UK), with data collected at an X-ray tube pressure of 40 kV and a tube current of 30 mA, and the scanning range ( $2\theta$ ) was 5–40°. The microscopic morphology of the samples was observed by scanning electron microscopy, using Hitachi S-4800 equipment (Tokyo, Japan) operating at 5 kV. The instrument used for the nitrogen adsorption experiments was a TriStar II 3020 from Micromeritics (Micromeritics, Norcross, GA, USA) at −196 °C. The equipment used for the mercury-pressure test was the AutoPore IV 9500 from Micromeritics (Norcross, GA, USA); Hg was filled into anode bulk samples of  $\approx 2.2$  g at pressures of  $3.45 \times 10^3$ – $4.14 \times 10^8$  Pa). The ammonia desorption tests were performed on equipment from Micromeritics, namely the model Autochem II 2920 (Micromeritics, Norcross, GA, USA), in which about 0.08 g of dried catalyst sample was loaded and heated to 150 °C to drive adsorbates off. Then, samples were cooled down in nitrogen and kept at 100 °C during ammonia adsorption and purging steps; the heating rate was 10 °C/min when the desorption started. The alumina contents were determined by XRF analysis using the Bruker AXS S4 spectrometer (Karlsruhe, Germany).

### 3.3. Catalytic Evaluation

The catalyst evaluation was carried out on a miniature fixed-bed reactor with a 14 mm inner diameter reaction tube, a catalyst charge of 1 g and a charge height of 4 cm. We used aqueous methanol as feedstock with a methanol mass content of 30% and a WHSV of  $2.0 \text{ h}^{-1}$  of methanol in the feed. The catalyst bed temperature was 480 °C and the reaction pressure was atmospheric. The evaluation test lasted for 24 h. Samples were taken every hour for analysis and the final average value was taken for comparison.

## 4. Conclusions

The product distribution of methanol conversion in ZSM-5 molecular sieve catalysts is the result of the joint primary and secondary reactions. The improvement of the selectivity to propylene depended on the effective inhibition of the secondary reaction. The acidic sites of molecular sieves are the catalytic activity centers of the primary and secondary multiple reactions. In the present work, as the content of alumina in the molecular sieve decreased, the selectivity of propylene increased in the products. At the same time, the selectivity of propane and other related by-products decreased. Moreover, the diffusion had an important influence on product distribution. The limitation of intracrystalline diffusion was enhanced with the increase of molecular sieve primary crystal size. Side reactions, such as hydrogen transfer reaction, oligomerization, aromatization and so on, were suppressed. As a result, the selectivity of propylene increased relatively. The combined effect of acid optimization and diffusion control maximized the propylene output.

**Author Contributions:** Methodology, W.Z. and X.Y.; Software, W.Z., K.W. and X.Y.; Validation, X.Y.; Investigation, K.W.; Resources, Y.G.; Data curation, X.G.; Writing—original draft, W.Z.; Writing—review and editing, X.G. and Y.G.; Supervision, Y.G. All authors have read and agreed to the published version of the manuscript.

**Funding:** This research was funded by National Key Research and Development Project (2022YFE0124100), the National Natural Science Foundation of China (grant nos. 21902054 and 22072049), Ordos Key Research and Development Project (2022EEDSKJZDZX003), and the Innovation and Talent Recruitment Base of New Energy Chemistry and Device (B21003). The authors also thank the HUST Academic Frontier Youth Team (grant no. 2019QYTD06).

**Data Availability Statement:** Data are contained within the article.

**Conflicts of Interest:** Authors Wei Zhang and Xiaojing Yong were employed by the company National Energy Group Ningxia Coal Industry. The remaining authors declare that the research was conducted in the absence of any commercial or financial relationships that could be construed as a potential conflict of interest.

## References

1. Haw, J.F.; Song, W.; Marcus, D.M.; Nicholas, J.B. The mechanism of methanol to hydrocarbon catalysis. *Acc. Chem. Res.* **2003**, *36*, 317–326. [[CrossRef](#)]
2. Ahmadi, S.M.A.; Askari, S.; Halladj, R. A review on kinetic modeling of deactivation of SAPO-34 catalyst during methanol to olefins (MTO) process. *Afinidad* **2013**, *70*, 130–138.
3. Wragg, D.S.; Akporiaye, D.; Fjellvag, H. Direct observation of catalyst behaviour under real working conditions with X-ray diffraction: Comparing SAPO-18 and SAPO-34 methanol to olefin catalysts. *J. Catal.* **2011**, *279*, 397–402. [[CrossRef](#)]
4. Dehertog, W.J.H.; Froment, G.F. Production of light alkenes from methanol on ZSM-5 catalysts. *Appl. Catal.* **1991**, *71*, 153–165. [[CrossRef](#)]
5. Chang, C.D.; Chu, C.T.-W.; Socha, R.F. Methanol conversion to olefins over ZSM-5: I. Effect of temperature and zeolite SiO<sub>2</sub>/Al<sub>2</sub>O<sub>3</sub>. *J. Catal.* **1984**, *86*, 289–296. [[CrossRef](#)]
6. Huang, H.-W.; Zhu, H.; Zhang, S.-H.; Zhang, Q.; Li, C.-Y. Effect of silicon to aluminum ratio on the selectivity to propene in methanol conversion over H-ZSM-5 zeolites. *J. Fuel Chem. Technol.* **2019**, *47*, 74–82. [[CrossRef](#)]
7. Palčić, A.; Ordonsky, V.V.; Qin, Z.; Georgieva, V.; Valtchev, V. Tuning zeolite properties for highly efficient synthesis of propylene from methanol. *Chem. A Eur. J.* **2018**, *24*, 13136–13149. [[CrossRef](#)]
8. Choi, M.; Na, K.; Kim, J.; Sakamoto, Y.; Terasaki, O.; Ryoo, R. Stable single-unit-cell nanosheets of zeolite MFI as active and long-lived catalysts. *Nature* **2009**, *461*, 246. [[CrossRef](#)]
9. Dybala, M.; Becker, P.; Trefz, D.; Klemm, E.; Fischer, A.; Jakob, H.; Hunger, M. Parameters influencing the selectivity to propene in the MTO conversion on 10-ring zeolites: Directly synthesized zeolites ZSM-5, ZSM-11, and ZSM-22. *Appl. Catal. A Gen.* **2016**, *510*, 233–243. [[CrossRef](#)]
10. Müller, S.; Liu, Y.; Kirchberger, F.M.; Tonigold, M.; Sanchez-Sanchez, M.; Lercher, J.A. Hydrogen transfer pathways during zeolite catalyzed methanol conversion to hydrocarbons. *J. Am. Chem. Soc.* **2016**, *138*, 15994–16003. [[CrossRef](#)]
11. Qiao, Q.; Wang, R.; Gou, M.; Yang, X. Catalytic performance of boron and aluminium incorporated ZSM-5 zeolites for isomerization of styrene oxide to phenylacetaldehyde. *Microporous Mesoporous Mater.* **2014**, *195*, 250–257. [[CrossRef](#)]
12. Yarulina, I.; Wispelaere, K.D.; Bailleul, S. Structure–performance descriptors and the role of Lewis acidity in the methanol-to-propylene process. *Nat. Chem.* **2018**, *10*, 804–812. [[CrossRef](#)] [[PubMed](#)]
13. Sundaramurthy, V.; Lingappan, N. Isomorphic substitution of boron in ZSM-5 type zeolites using TBP as template. *J. Mol. Catal. A Chem.* **2000**, *160*, 367–375. [[CrossRef](#)]
14. Saravi, F.Y.; Taghizadeh, M. Synergetic effect of Mn, Ce, Ba, and B modification and moderate desilication of nanostructured HZSM-5 catalyst on conversion of methanol to propylene. *Turk. J. Chem.* **2018**, *42*, 1640–1662. [[CrossRef](#)]
15. Schulz, H. “Coking” of zeolites during methanol conversion: Basic reactions of the MTO-, MTP- and MTG processes. *Catal. Today* **2010**, *154*, 183–194. [[CrossRef](#)]
16. Yang, Y.; Sun, C.; Du, J.; Yue, Y.; Hua, W.; Zhang, C.; Shen, W.; Xu, H. The synthesis of enduring B-Al-ZSM-5 catalysts with tunable acidity for methanol to propylene reaction. *Catal. Commun.* **2012**, *24*, 44–47. [[CrossRef](#)]
17. Yang, Z.; Xia, Y.; Mokaya, R. Zeolite ZSM-5 with unique supermicropores synthesized using mesoporous carbon as a template. *Adv. Mater.* **2004**, *16*, 727–732. [[CrossRef](#)]
18. Yaripour, F.; Shariatnia, Z.; Sahebdehfar, S.; Irandoukht, A. Effect of boron incorporation on the structure, products selectivities and lifetime of H-ZSM-5 nanocatalyst designed for application in methanol-to-olefins (MTO) reaction. *Microporous Mesoporous Mater.* **2015**, *203*, 41–53. [[CrossRef](#)]
19. Almutairi, S.M.T.; Mezari, B.; Pidko, E.A.; Magusin, P.C.M.M.; Hensen, E.J.M. Influence of steaming on the acidity and the methanol conversion reaction of HZSM-5 zeolite. *J. Catal.* **2013**, *307*, 194–203. [[CrossRef](#)]
20. Ding, C.; Wang, X.; Guo, X.; Zhang, S. Characterization and catalytic alkylation of hydrothermally dealuminated nanoscale ZSM-5 zeolite catalyst. *Catal. Commun.* **2008**, *9*, 487–493. [[CrossRef](#)]
21. Vu, D.V.; Miyamoto, M.; Nishiyama, N.; Ichikawa, S.; Egashira, Y.; Ueyama, K. Catalytic activities and structures of silicalite-1/H-ZSM-5 zeolite composites. *Microporous Mesoporous Mater.* **2008**, *115*, 106–112. [[CrossRef](#)]
22. Anderson, J.R.; Mole, T.; Christov, V. Mechanism of some conversion over ZSM-5 zeolite. *J. Catal.* **1980**, *61*, 477–484. [[CrossRef](#)]

23. Öhrman, O.; Hedlund, J.; Msimang, V.; Möller, K.; Sterte, J. ZSM-5 structured catalysts coated with silicalite-1. *Stud. Surf. Sci. Catal.* **2004**, *154*, 677–684.
24. Ono, Y.; Mori, T. Mechanism of methanol conversion into hydrocarbons over ZSM-5 zeolite. *J. Chem. Soc. Faraday Trans. 1 Phys. Chem. Condens. Phases* **1981**, *77*, 2209. [[CrossRef](#)]
25. Chen, G.; Jiang, L.; Wang, L.; Zhang, J. Synthesis of mesoporous ZSM-5 by one-pot method in the presence of polyethylene glycol. *Microporous Mesoporous Mater.* **2010**, *134*, 189–194. [[CrossRef](#)]
26. Mikkelsen, Ø.; Rønning, P.O.; Kolboe, S. Use of isotopic labeling for mechanistic studies of the methanol-to-hydrocarbons reaction. Methylation of toluene with methanol over H-ZSM-5, H-mordenite and H-beta. *Microporous Mesoporous Mater.* **2000**, *40*, 95–113. [[CrossRef](#)]
27. Cui, N.; Guo, H.; Zhou, J.; Li, L.; Guo, L.; Hua, Z. Regulation of framework Al distribution of high-silica hierarchically structured ZSM-5 zeolites by boron-modification and its effect on materials catalytic performance in methanol-to-propylene reaction. *Microporous Mesoporous Mater.* **2020**, *306*, 110411. [[CrossRef](#)]
28. Shen, Y.; Liang, H.; Liao, Z.; Jiang, B.; Wang, J.; Yang, Y.; Li, M.; Luo, Y.; Shu, X. Pore plugging effects on the performance of ZSM-5 catalyst in MTP reaction using a discrete model. *Chin. J. Chem. Eng.* **2021**, *32*, 253–263. [[CrossRef](#)]
29. Wu, J.; Wang, C.; Meng, X.; Liu, H.; Chu, R.; Wu, G.; Li, W.; Jiang, X. Enhancement of catalytic and anti-carbon deposition performance of SAPO-34/ZSM-5/quartz films in MTA reaction by Si/Al ratio regulation. *Chin. J. Chem. Eng.* **2023**, *56*, 314–324. [[CrossRef](#)]

**Disclaimer/Publisher's Note:** The statements, opinions and data contained in all publications are solely those of the individual author(s) and contributor(s) and not of MDPI and/or the editor(s). MDPI and/or the editor(s) disclaim responsibility for any injury to people or property resulting from any ideas, methods, instructions or products referred to in the content.